Inorganic Chemistry

pubs.acs.org/IC Article

Influence of Internal Angular Arrangement on Pnicogen Bond Strength

Steve Scheiner,* Mariusz Michalczyk, and Wiktor Zierkiewicz



Cite This: Inorg. Chem. 2023, 62, 20209-20218



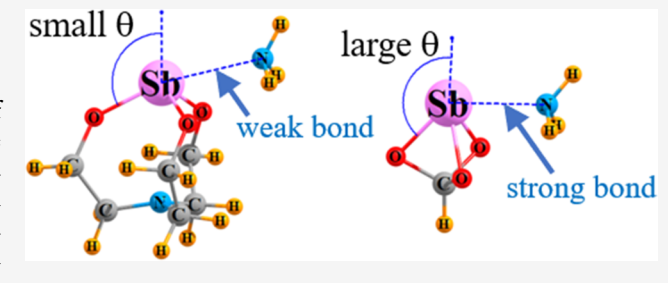
ACCESS I

III Metrics & More

Article Recommendations

Supporting Information

ABSTRACT: The three Z–X covalent bonds of a ZX₃ unit (Z = P, As, Sb, Bi) are normally arranged in a pyramidal structure. Quantum chemical calculations show that pnicogen bonds (ZBs) to the central Z are weakened if ZX₃ is flattened, as in the opening of an umbrella. The partial closing of the umbrella has the opposite effect of substantially strengthening these ZBs, even amounting to a 2- or 3-fold magnification in certain cases. The strongest such bonds, wherein Sb and Bi are in a strained configuration within a ZO_3CH model system, have interaction energies of 20 kcal/mol with an NH₃ base. Most of these systems, whether flattened or



more pyramidal, are capable of engaging in three ZBs simultaneously, despite a certain amount of negative cooperativity.

INTRODUCTION

A number of close relatives of the intensively studied Hbond¹⁻⁶ have been under intense scrutiny in recent years. These noncovalent bonds replace the bridging proton with any of a wide array of other atoms, many of which are more electronegative than H.7-16 Although these atoms cannot be characterized as carrying an overall partial positive charge as does a bridging H, each such A atom nonetheless possesses a region of positive molecular electrostatic potential (MEP) that lies along the extension of the R-A covalent bond. 17-27 Since it owes its existence to the depletion of electron density in this area, this positive region is often denoted as a σ -hole. Just as in the case of the HB, this σ -hole can attract a nucleophile, leading to the classification of these interactions under the general rubric of σ -hole bonds. However, there is a tendency to subclassify each such bond according to the family from which is drawn the bridging atom that substitutes for H. So, for example, halogen bonds utilize Cl, Br, and I, while S, Se, and Te are involved in chalcogen bonds, and so on. 24,28-

The pnicogen bond (ZB) is particularly interesting in that the central Z atom is commonly trivalent, as in ZX₃, where Z represents a pnicogen atom (P, As, Sb, Bi) and X represents any of a wide selection of substituents. The presence of three Z–X covalent bonds, usually arranged in a pyramidal shape, leads to three σ -holes, all of which can potentially engage in a ZB with an incoming nucleophile. This sort of bond has generated a great deal of interest, and the ensuing research 15,34–40 has led to a number of overarching principles that guide the strength and properties of these bonds. In the first place, the σ -hole deepens as the Z atom moves down in the periodic table (P < As < Sb < Bi) due to its growing electropositivity and polarizability. A similar phenomenon occurs as the X substituents grow more electron-withdrawing,

again deepening the σ -hole on the Z and strengthening the ensuing ZB with a nucleophile. Like the other related noncovalent bonds of this type, ZBs seldom contain a first-row atom, in this case N, as the Lewis acid atom, due in large measure to its high electronegativity, which resists σ -hole formation. Although the presence of one such ZB inhibits the formation of a second such bond to the same Z atom due to negative cooperativity, the tendency toward such bonding is sufficiently compelling that two, three, and even more such bonds have been observed. $^{41-49}$

As mentioned above, the three covalent bonds around the trivalent Z atom in a ZX_3 motif are typically disposed in a pyramidal shape as in PCl_3 , for example. However, the precise angle between these bonds can be heavily influenced by the internal strains that are introduced when the Z atom is part of a cage molecule. In particular, Cozzolino and others have synthesized and characterized systems where a heavy Z atom is connected to three O atoms, which are in turn bonded to other segments of an overall cage framework that places certain strains on the ZO_3 connector. On one extreme lies the atranes, which contain three five-membered rings, with Z serving as a bridgehead atom. The overall structure pulls up on the three O atoms, flattening the ZO_3 arrangement to some degree. The opposite effect occurs with smaller rings that pull down on the O atoms, making this motif more pyramidal.

Received: September 7, 2023 Revised: November 16, 2023 Accepted: November 20, 2023 Published: November 28, 2023





What is of special interest is the effect that this adjustable degree of pyramidality might exert on the pnicogen bonds that this central Z atom may form with nucleophiles. Previous work has demonstrated that such ZBs are indeed possible and are present in the crystalline forms of these molecules. Indeed, full occupation of all three σ -holes surrounding a given Z atom seems to be the norm. The large question then is whether the flattening of the C_3 -symmetric ZO $_3$ unit exerts any effect upon the strengths of these ZBs, and if so, to what extent. This work attempts to directly address this question by quantum chemical calculations of systems specifically chosen for this purpose. Varying degrees of pyramidality are imposed on a central pnicogen atom first artificially on small model molecules and then by designing others in which the strain is part and parcel of their internal structure.

METHODS

Quantum chemical calculations were carried out with the aid of the Gaussian 16^{56} program. The M06-2X functional was applied in the context of the def2-TZVPP basis set, which includes a triple- ζ foundation, and designed so as to include certain relativistic effects. This function has been repeatedly assessed to be one of the most accurate for interactions such as those considered here. S8-65 Geometries were fully optimized and verified as true minima by the lack of any imaginary vibrational frequencies, with the exception of those systems where certain internal angles were imposed.

The interaction energy $E_{\rm int}$ is formulated as the difference between the energy of each complex and the sum of the energies of the two subunits in the geometry they adopt within the complex. $E_{\rm int}$ was corrected for basis set superposition error by the counterpoise formalism. ⁶⁶ The Multiwfin program ⁶⁷ located the extrema of the molecular electrostatic potential (MEP) on the $\rho=0.001$ au isodensity surface of each monomer. The density of each bond critical point was measured in the context of the QTAIM protocol ⁶⁸ using the AIMALL program. ⁶⁹ The energetic effects of interorbital charge transfer were evaluated by the NBO procedure. ^{70,71} Symmetry adapted perturbation theory (SAPT) ^{72,73} evaluated various components that contribute to the interaction energies via the PSI4 program. ⁷⁴

RESULTS

Externally Imposed Deformations. As a first step in understanding the connection between internal geometry and pnicogen bond strength, a number of simple ZX₃ Lewis acids were considered, where Z refers to P, As, Sb, and Bi, and X designates F, Cl, or OH. Geometrical distortions were imposed on each Lewis acid as described below.

Characterization of Lewis Acid Monomers. The definitions of the umbrella angle θ and the internal angle α of each ZX₃ molecule are presented in Figure 1. The broken blue line represents the C_3 rotation axis, in this case of SbCl₃. As θ increases, the molecule closes like an umbrella; therefore, θ is referred to here as the umbrella angle. The internal angles between the two substituents and the central atom are defined as α . In the extreme case of a fully planar molecule with θ = 90°, α would be 120°, whereas both angles would be equal to 109.5° if the molecules were to adopt a fully tetrahedral geometry as another extreme. The optimal umbrella angles for the ZX₃ units chosen for study are contained in Table S1, along with the associated internal angles, where it may be seen that the umbrella angles all lie within a span of 2 of 120°, leaving α in the 94–100° range. These computationally optimized geometries are quite close to those that have been experimentally determined in the gas phase as is evident in Table S2.

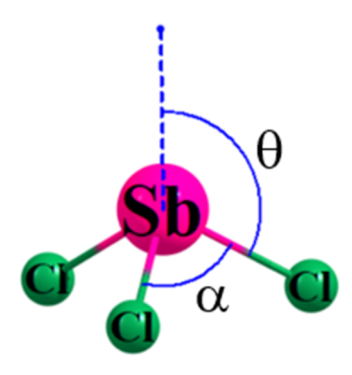


Figure 1. Definition of internal angles within ZX_3 molecules using $SbCl_3$ as an example. The broken blue line refers to the C_3 rotation axis.

The molecular electrostatic potential (MEP) of each of these acids is exemplified by the Bi series in Figure 2 where the blue

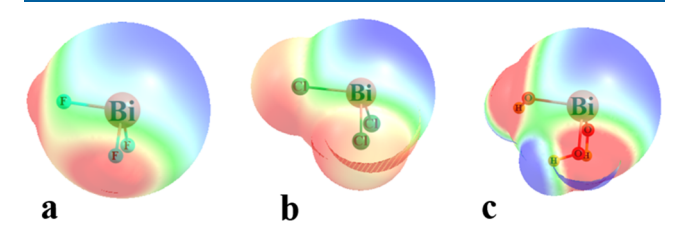


Figure 2. Molecular electrostatic potential surrounding the BiX_3 series. Blue and red regions indicate positive and negative MEPs; values are (a) + 38, -31, (b) + 31, -13, and (c) + 19, -13 kcal/mol.

and red regions, respectively, indicate the positive and negative potentials. A positive blue region, or σ -hole, lies directly opposite each of the substituents, lying within 10° of the projection of the X-Bi axis. Inspecting the middle column of Table 1, which refers to the fully optimized monomer, it is

Table 1. $V_{\rm max}$ (kcal/mol) Computed for Deviations of θ from Its Optimized Value

	-20°	-10°	0°	+10°	+20°
PF_3	6.3	25.0	28.3	41.6	47.6
PCl ₃	7.4	13.6	21.4	30.0	38.1
$P(OH)_3^a$		-13.3	-4.5	6.6	34.6
AsF_3	22.7	30.7	40.6	49.9	55.6
$AsCl_3$	15.2	21.8	29.9	37.9	44.7
$As(OH)_3^a$		-0.7	14.9	27.4	36.5
SbF ₃	31.6	40.2	50.1	58.8	64.0
SbCl ₃	25.6	32.6	40.9	48.8	55.0
$Sb(OH)_3^a$		11.1	30.7	37.0	45.7
BiF_3	51.8	53.0	60.8	68.1	72.7
$BiCl_3$	47.8	48.3	54.1	60.0	64.6
$Bi(OH)_3$	16.7	25.5	39.8	46.2	55.5
Average of th	ree σ -holes.				

apparent that the value of $V_{\rm max}$ that characterizes this σ -hole diminishes in the X sequence F > Cl > OH. At the same time, the σ -hole deepens as the central Z atom grows larger, reaching a maximum of 60.8 kcal/mol for BiF₃.

With regard to the behavior of the σ -hole as the umbrella angle changes, the values of $V_{\rm max}$ are reported in Table 1 for steps of θ by 10° in either direction. As may be seen, larger values of θ , corresponding to a closing of the umbrella, deepen

these σ -holes, while a diminishing θ associated with a flatter molecule weakens the holes. These changes can be substantial. Taking SbCl₃ as an example, its optimized $V_{\rm max}$ of 40.9 kcal/mol increases by 34% upon an increase of θ by 20°, whereas a reduction of θ by the same amount weakens the σ -hole by roughly the same percentage. It might be noted that the σ -holes seem to disappear for most of the trihydroxy units, with the exception of Bi(OH)₃, and is even negative in sign for the smaller θ angles of P(OH)₃. As the molecule flattens out, these three σ -holes indeed disappear, morphing into a single positive region that lies above the incipient molecular plane.

A full characterization of the MEP surrounding each of these units should also include the minimum that occurs along the C_3 axis, corresponding to the position of the Z lone pair. Unlike a molecule like NH_3 , the minima of these ZX_3 molecules tend to be positive in sign. This distinction is due first to the lesser electronegativity of the Z atoms as compared to that of N. The second factor is the electron-withdrawing power of the three X substituents. Both of these effects are fully evidenced in Table 2 where V_{\min} becomes more positive as Z

Table 2. V_{\min} (kcal/mol) Lying along the Principal C_3 Rotation Axis Computed for Deviations of θ from Its Optimized Value

	-20°	-10°	0°	+10°	+20°
PF ₃	-13.9	-8.3	3.1	20.6	32.8
PCl_3	-12.6	-6.2	4.0	15.5	28.0
$P(OH)_3$	-42.0	-32.3	-19.0	-4.7	10.2
AsF_3	0.4	6.6	18.8	30.3	39.7
AsCl ₃	2.1	5.4	14.2	24.0	34.2
$As(OH)_3$	-29.8	-19.8	-3.4	8.2	22.7
SbF_3	15.7	19.3	27.9	36.2	43.1
SbCl ₃	12.9	15.5	22.9	31.0	39.6
$Sb(OH)_3$	-14.4	-6.7	6.4	15.8	27.3
BiF_3		49.3	52.7	56.0	58.8
$BiCl_3$		43.6	46.8	51.2	56.4
Bi(OH) ₃	13.0	17.6	27.4	34.3	43.1

grows larger and less electronegative. This trend is fairly dramatic: taking the optimized geometries of the ZF₃ series as an example, $V_{\rm min}$ grows from 3.1 kcal/mol for PF₃ all the way up to 52.7 kcal/mol for BiF₃. Just as for the σ -holes, $V_{\rm min}$ also grows more positive as θ increases, and the molecule becomes more pyramidal.

Complexes with NH₃. When an NH₃ base molecule is allowed to interact with each of these Lewis acid molecules, it aligns with one of the σ -holes. Typical examples of these dyads are displayed in Figure 3 for the Sb series. The energetics of the resulting dyads are listed in Table 3 where it is immediately obvious that these pnicogen bonds are fairly strong. Interaction energies vary between 8 and 17 kcal/mol. The binding energies $E_{\rm b}$, which also take account of monomer deformations to

achieve the geometry within the complex, are only slightly smaller, consistent with only minor internal geometrical changes. Consistent with expectations and the σ -hole depths outlined above, these bonds grow stronger as the Z atom is enlarged from P to As to Sb to Bi. For each Z atom, it is ZF₃ that engages in the strongest bond, which matches its deepest σ -hole. However, although the ZCl₃ hole is consistently deeper than that of Z(OH)₃, the interaction energies are fairly similar. This near-equality may be due to the presence of weak H-bonds, which provide additional stabilization for the complexes containing the hydroxyl groups (see below).

The bond critical point densities in the next column of Table 3 are generally consistent with the energetics but not entirely. For example, these quantities do not all follow the energetic pattern of P < As < Sb < Bi. Three of the $Z(OH)_3$ complexes contain HB bond paths that supplement ZB and inflate the total interaction energy; both are reported in Table 3 for clarity. The same partial inconsistency applies to the NBO measures of charge-transfer energy in the next column of the table. The E_2 quantity refers to the second-order perturbation energy associated with the transfer of charge from the NH₃ lone pair to the pertinent $\sigma^*(ZX)$ antibonding orbital of the Lewis acid. E_2 is the largest for Sb, and the F substituent does not have the largest E_2 . The aforementioned HBs within complexes of $Z(OH)_3$ add a small amount to this measure of bond strength.

As a base is added to any of these ZX₃ units, there is a tendency for this fourth ligand, as it were, to draw the geometry away from a simple trigonal pyramid and toward a more "seesaw" shape, with the Z lone pair acting as the fifth electron domain within a trigonal bipyramid framework. A pure geometry of this sort would place the apical units 180° from one another, with 90° angles separating the apical from equatorial. The approach of the $\theta(X_{ap}Z\cdots N)$ angles listed in Table 3 toward 180° can be used as a gauge of the partial transformation toward such a seesaw arrangement, just as can the $\theta(X_{ap}ZX)$ angles as they approach 90°.

The geometrical features of these complexes can be compared to the available structural data. Taking AsCl₃ as an example, its As–Cl bond lengths in the solid phase ⁷⁶ are 2.161 Å, quite close to the 2.169 Å computed here for the monomer. Pairing this Lewis acid with NMe₃ stretched these bonds, particularly that directly opposite the base, consistent with our geometrical adjustments noted with the NH₃ base, where the elongation of that N–Cl bond was twice that of the other two bonds. This greater elongation is carried over⁷⁷ to the pnicogen-bonded complex between SbCl₃ and PhNH₂. Regarding angular aspects, the $\theta(X_{ap}Z\cdots N)$ and $\theta(X_{ap}ZX)$ angles are measured to be 178.7 and 91.6°, respectively, somewhat closer to a trigonal bipyramid, in line with the stronger basicity of NMe₃, as well as the change in phase from gas to crystalline.

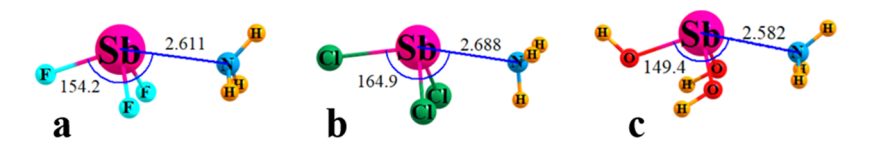


Figure 3. Optimized geometries of NH_3 with (a) SbF_3 , (b) $SbCl_3$, and (c) Sb ($OH)_3$. Distances in Å, angles in degs. The minima display small differences in conformation in that the NH_3 is eclipsed with respect to SbX_3 in panels (a, c), while it is staggered for panel (b); these are the only minima for each dyad with the exceptions of PF_3 and AsF_3 where the two minima have nearly identical energies.

Table 3. Energetics of Complexes of ZX₃ with NH₃ (kcal/mol), Z···N Bond Critical Point Density (au), NBO Charge-Transfer Energy (kcal/mol), and Bond Angles (degs) to the Apical X_{ap} Atom

	$-E_{ m int}$	$-E_{\rm b}$	$ ho_{ ext{BCP}}$	E_2^{a}	$\theta(X_{ap}Z\cdots N)$	$\theta(X_{ap}ZX)$
PF ₃	5.62	5.28	0.019	2.82	166.7	95.5
PCl ₃	5.47	5.12	0.019	8.36	177.1	98.2
$P(OH)_3$	2.68	2.40	$0.028^{b} (0.009)$	$1.90^d (0.87)$	160.0	93.7
AsF_3	10.20	9.40	0.030	13.83	162.3	92.5
$AsCl_3$	8.36	7.73	0.025	17.65	172.8	96.1
$As(OH)_3$	8.89	7.14	0.028	14.35	157.9	91.7
SbF ₃	15.86	14.51	0.041	22.80	154.4	89.9
SbCl ₃	13.15	12.05	0.026	25.72	165.0	93.5
$Sb(OH)_3$	14.98	12.33	$0.030^{b} (0.012)$	27.36^{c} (26.86)	149.1	87.8
BiF_3	17.33	16.31	0.033	17.76	153.5	90.8
$BiCl_3$	15.19	14.45	0.029	21.84	168.5	95.4
$Bi(OH)_3$	15.97	13.45	$0.042^{b} (0.010)$	20.32^d (19.47)	146.5	90.2

 $^aN_{LP} \rightarrow \sigma^*(Z-X)$. bSum of BCPs of ZX and additional HBs (BCP for ZB in parentheses). cSum of E_2 for $N_{LP} \rightarrow \sigma^*(Z-X) + N_{LP} \rightarrow \sigma^*(O-H)$. dSum of E_2 for $N_{LP} \rightarrow \sigma^*(Z-X) + N_{LP} \rightarrow \sigma^*(O-H) + O_{LP} \rightarrow \sigma^*(N-H)$.

Just as it was found above that the σ -holes lying opposite the three X substituents grow larger as the ZX₃ unit adopts a more pyramidal shape, so too does the associated ZB become stronger. Table 4 reports the interaction energy between NH₃

Table 4. Interaction Energy ($-E_{\rm int}$, kcal/mol) of NH₃ with the σ -Hole of the Indicated Lewis Acid for Deviations of θ from Its Optimized Value

	-20°	-10°	0°	+10°	+20°
PF ₃		3.61	5.05	10.44	15.69
PCl ₃		2.72	4.85	7.88	12.41
$P(OH)_3$			2.25	4.30	7.69
AsF_3	3.13	5.27	8.77	13.48	18.28
AsCl ₃	3.45	4.88	7.29	10.45	14.28
$As(OH)_3$			3.67	7.93	10.97
SbF ₃	6.87	9.41	13.51	18.25	22.70
SbCl ₃	6.66	8.26	11.18	14.75	18.59
$Sb(OH)_3$	9.29	8.71	8.17	11.00	15.52
BiF_3	12.41	12.65	15.54	19.31	22.84
BiCl ₃	15.04	12.24	13.83	16.32	19.01
$Bi(OH)_3$	6.22	7.55	10.51	14.37	19.09

and ZX₃ when the umbrella angle of the monomer is held at a predefined value, in $\pm 10^\circ$ increments away from the angle within the monomer. In line with the increasing $V_{\rm max}$ as the Lewis acid takes on a more pyramidal shape, so too does the interaction energy increase with an approaching base. These energetics are fairly sensitive to this internal angle; for example, a 20° increase in θ increases the interaction energy by some 5.2–9.5 kcal/mol, which can amount to as much as a doubling or even a tripling of the quantity without any change imposed on the monomer's preferred geometry. Note that the reverse effect of a ZB weakening occurs as θ diminishes, and the acid molecule flattens out. Indeed, some of the weaker ZBs disappear for flatter manifestations of these acids.

Much of what occurs in terms of bond energies manifests itself as well in the AIM bond critical point densities contained in Table S3. These densities increase with an increasing pyramidal character, varying in the range between 0.012 and 0.050 au. The increase in the NBO E_2 measure of charge transfer is even more dramatic. As reported in Table S4, this perturbation energy for transfer from the NH₃ lone pair to the $\sigma^*(ZX)$ antibonding orbital ranges from a minimum of only

0.4 kcal/mol up to as much as 32 kcal/mol when θ has increased by 20°. The behavior of E_2 for the Sb(OH)₃ system is a bit anomalous in this regard, with maxima at either extremum.

Given the large changes in the interaction energy occurring upon pyramidalization of ZX3, one might wonder if the character of the bond might be changing. Table S5 lists each of the components, as well as their percentage contribution to the total attractive component, as evaluated by SAPT. Taking the undistorted $\Delta\theta = 0^{\circ}$ first, electrostatics (ES) generally accounts for the largest share of the total, accounting for 45-64% of the total. The share attributed to induction (IND) is quite variable, generally larger for the heavier Z atoms, where it can rival ES. Dispersion (DISP) is also variable, about 30% for several complexes but diminishing to less than 10% for the larger Z atoms. The repulsive exchange energy, which keeps the two subunits from collapsing into one another, has been shown to represent an important aspect of the angular features of various sorts of noncovalent bonds including pnicogen bonds. 78,79 This component is largest for the halogen substituents and quite a bit smaller for OH and grows quickly along with the size of the central Z atom. A scan of all of the θ angles in Table S5 suggests that these fractional contributions are relatively stable, such that there is no evidence of any fundamental change in the contributing factors as the Lewis acid distorts. The exchange energy grows increasingly repulsive as the molecule becomes more pyramidal, and the θ angle

The effect of the changing umbrella angle upon the dyad geometries is particularly interesting. Figure 4 contains a slide presentation depicting the changing intermolecular distances and orientations for the BiF₃ case, as an example. When the molecule has flattened out so that θ is 20° below its optimized value, the NH₃ lies some 50° away from the BiF₃ C₃ rotation axis, as exhibited in Figure 4a. As θ is increased, this angle progressively widens to 79° at the optimal umbrella angle, as shown in Figure 4c. As BiF₃ continues to become more pyramidal, the NH_3 is displaced further from the C_3 axis, ultimately lying 90° from this axis after a 20° deformation in Figure 4e. It may be noted as well that the intermolecular Bi---N distance shortens as θ increases and the ZB energy increases. Another geometric parameter of some interest is the FBi···N angle, which is associated with the ability of the N lone pair to align with the relevant $\sigma^*(BiF)$ orbital. This angle maximizes at

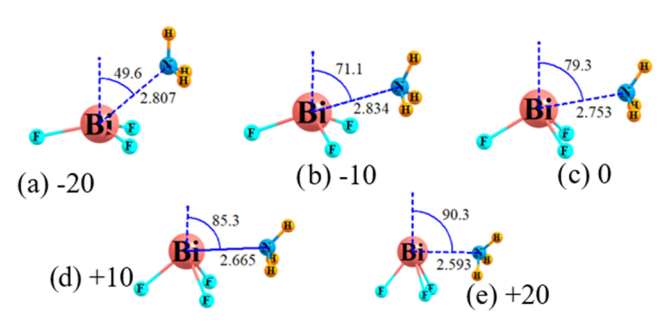


Figure 4. Geometries of $F_3Bi\cdots NH_3$ complexes for various deviations of θ from its optimal angle by (a) -20° , (b) -10° , (c) optimal, (d) $+10^\circ$, and (e) $+20^\circ$. The local C_3 rotation axis of BiF₃ is shown as a broken blue line. Distances in Å, angles in degs.

177 for a 10° decrement of θ from its optimal value and decreases as θ changes in either direction. More specifically, this angle is equal to 152, 177, 159, 143, and 128° for the (a–e) sequence depicted in Figure 4.

Internal Strain. It is of interest to apply the above principles to a real molecule, where the strain is not artificially imposed but is a product of the chemical bonding within. There have been several such molecules synthesized and studied to date. The stibatrane molecule designed by Moaven et al. 45 situates three internal five-membered rings into a cage as illustrated in Figure 5a. The prototypical example of a unit with no internal strain is Bi(OH)₃ in Figure 5b. Table 5 shows that the atrane rings have a flattening effect on the coordination around the central Bi, making the umbrella angle θ smaller than it might otherwise be. This decrease in θ is nearly 20° for Z=Bi, and it diminishes down to only 2° for P. The rings are smaller within the Bi(OCH₂)₃CH cage in Figure 5c, 43 so a certain degree of deformation is plausible, although this strain is small, increasing θ by less than 5° according to Table 5. In order to simulate numerous pnicogen-containing systems in the literature, which are more highly pyramidal, 80-85 the methylene groups were removed, as in Figure 5d, leading to shorter 3-atom Z-O-C chains. This greater strain increases the θ umbrella angle by some 15°, as indicated in the final column of Table 5, and an associated 25° decrease in the internal α angle.

Table 5. Internal Angles (deg) within Monomers along with the σ -Hole Depths on the Z Atom (kcal/mol) and the Orientation Angles β of $V_{\rm max}$ Relative to the OZ Axis, Calculated at the M06-2X/def2-TZVP Level

Z	Z-atrane	$Z(OH)_3$	Z(OCH ₂) ₃ CH	ZO ₃ CH
		θ	, 2,0	
Р	116.0	118.1	118.2	132.4
As	116.3	120.1	120.6	136.0
Sb	110.9	121.2	125.5	139.7
Bi	103.2	121.8	124.8	141.5
2.	100.2	α	12 110	1110
P	100.7	99.6	99.4	79.5
As	103.5	97.0	96.4	74.0
Sb	114.3	95.6	92.6	68.2
Bi	99.7	94.8	90.6	65.2
2.	<i>,,,,</i>	$V_{ m max}$	70.0	00.2
Р	-5.3	7.0	-3.2	26.9
As	7.1	19.2	11.3	39.6
Sb	12.6	33.4	25.1	51.2
Bi	24.7	39.8	37.3	59.2
2.	21.7	$\beta(OZ\cdots V)$		07.2
Р	168.0	163.4	169.1	159.5
As	166.3	162.4	170.2	152.8
Sb	169.8	164.3	166.2	147.0
Bi	167.0	167.6	172.4	148.2
DI	107.0	107.0	1/2.7	170.2

The $V_{\rm max}$ section of Table 5 fully conforms to the ideas emanating from the systems in the previous section, where the pyramidalization around the central Z atom was artificially imposed. The flattening of the ZO₃ arrangement in the atranes reduces $V_{\rm max}$ relative to undistorted Z(OH)₃, while the increased pyramidalization of ZO₃CH yields a sizable deepening of the σ -hole. Despite the small increases of θ in Z(OCH₂)₃CH, there is a small drop in $V_{\rm max}$ that is likely due to the electron donation from the alkyl groups. The full spectrum of the deepening of the σ -hole as the arrangement around the central Bi atom becomes more pyramidal is on full display in Figure 5e–5h, where the region to the right of this atom grows progressively bluer. As a final issue connected with these monomers, the lowermost section of Table 5 designates the position of the σ -hole via the β angle it makes with the OZ

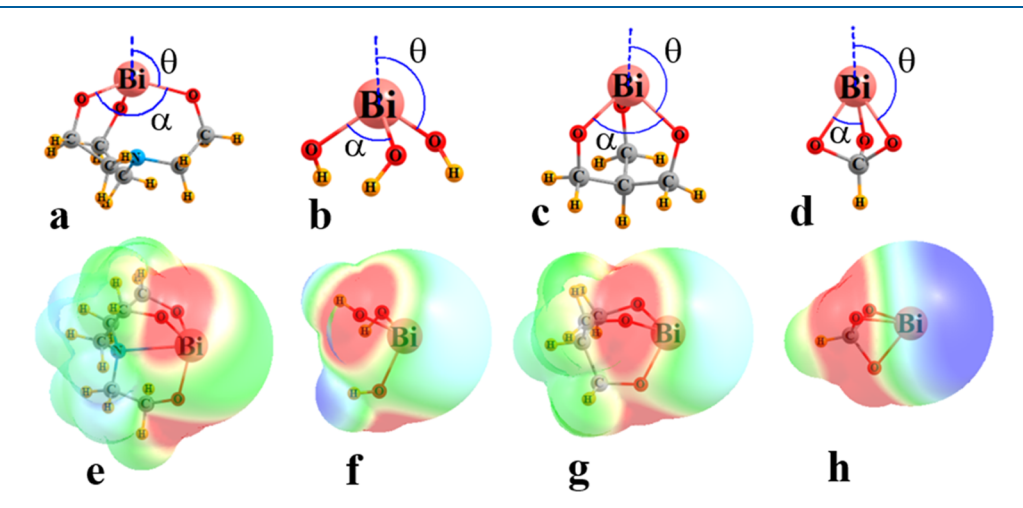


Figure 5. (a–d) Definitions of internal angles within Lewis acids with Z \equiv Bi. The broken blue line indicates the C_3 rotation axis of molecule. (e–h) MEP surrounding each molecule on the surface corresponding to 1.5 × vdW radii. Blue and red regions refer, respectively, to +30 and -20 kcal/mol.

bond axis with which it is connected. These angles are smaller than 180° , as is common with ZR_3 molecules where the Z lone pair tends to push the MEP maximum away from the C_3 axis. This discrepancy from linearity is most sizable for the highly strained ZO_3CH molecules, where β hovers around 150° .

These σ -holes attract an NH $_3$ nucleophile, and the geometries of the addition of one such base molecule to each of the systems in Figure 5 are depicted in Figure 6, again

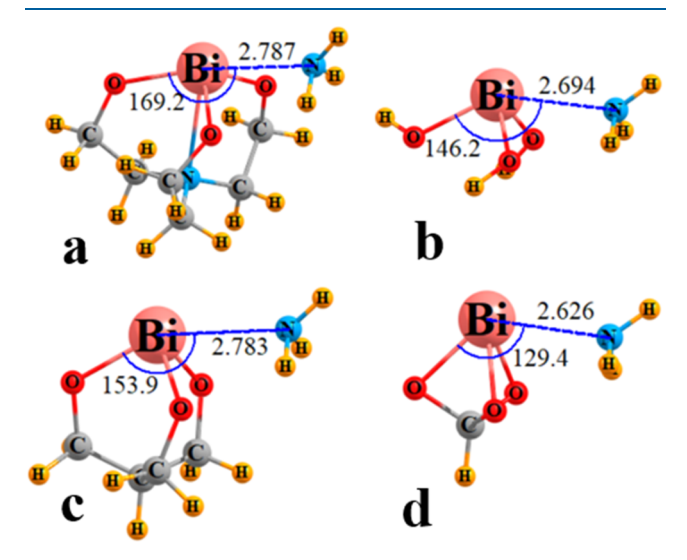


Figure 6. Optimized geometries of complexes containing NH₃ and the Lewis acids (a) biatrane, (b) Bi(OH)₃, (c) Bi(OCH₂)₃CH, and (d) BiO₃CH. Distances in Å and angles in degs.

for Z=Bi. It may be first noticed that the R(Bi···N) intermolecular separation decreases as the molecule becomes more pyramidal, which is consonant with the bond strengthening. The OBi···N angle decreases as well, as the N tends to follow along with the displacement of $V_{\rm max}$ as the Lewis acid becomes more pyramidal. One may note as well that there is a reversal in these trends between Figure 6b,c where the internal strain is little changed but the alkyl groups weaken the σ -hole.

As observed in crystals, these trivalent $Z(OR)_3$ units are not limited to only a single ZB. Indeed, each of the three σ -holes

on Z is capable of sustaining a ZB interaction with a base simultaneously. The structures of the complexes with 2 and 3 NH₃ units are depicted in Figure 7 for the Bi systems. Each addition of another base tends to slightly elongate the ZBs that are present due to the negative cooperativity, along with a small enlargement of the C_3 -Bi-N angles as the system flattens out a bit. There are, however, some exceptions. The σ -holes of the As-atrane molecule, with $V_{\rm max}=7.1$ kcal/mol, are too shallow to allow more than a single ZB. And with their very shallow σ -holes, with the exception of PO₃CH, the P-acids are incapable of sustaining even one ZB, much less multiple bonds. Even the atranes of the larger Z atoms show signs of ZBs breaking down. Note, for example, the asymmetry of the two Bi··N distances in Figure 7a.

Most importantly, the energetics of these ZBs obey the ideas enunciated above in that the ZBs strengthen as the coordination of the central Z atom transitions from flat to more pyramidal. Table 6 lists the interaction energy of each

Table 6. Average Interaction Energy for n NH₃ Units (Total $-E_{\text{int}}$)/n (kcal/mol)

		, ,	,	
Z	Z-atrane	$Z(OH)_3$	$Z(OCH_2)_3CH$	ZO_3CH
		n = 1		
P				9.13
As	3.90	5.75 ^a	4.96	14.13
Sb	9.75	15.25	10.22	19.55
Bi	11.63	16.22	12.95	20.31
		n = 2		
P				7.71
As		5.38 ^a	4.94	12.23
Sb	8.22	10.35	9.98	17.81
Bi	11.06	13.33	13.19	19.55
		n = 3		
P				7.10
As		5.09 ^a	5.91	10.99
Sb	7.62	9.49	9.67	16.27
Bi	10.33	12.80	13.34	18.87
^a Restrict	HOAsO dihee	dral angles.		

complex for P, As, Sb, and Bi, divided by the number of ZBs present, so as to extract the average bond energy. The lowest interaction energies arise in the flat atranes, progress to larger

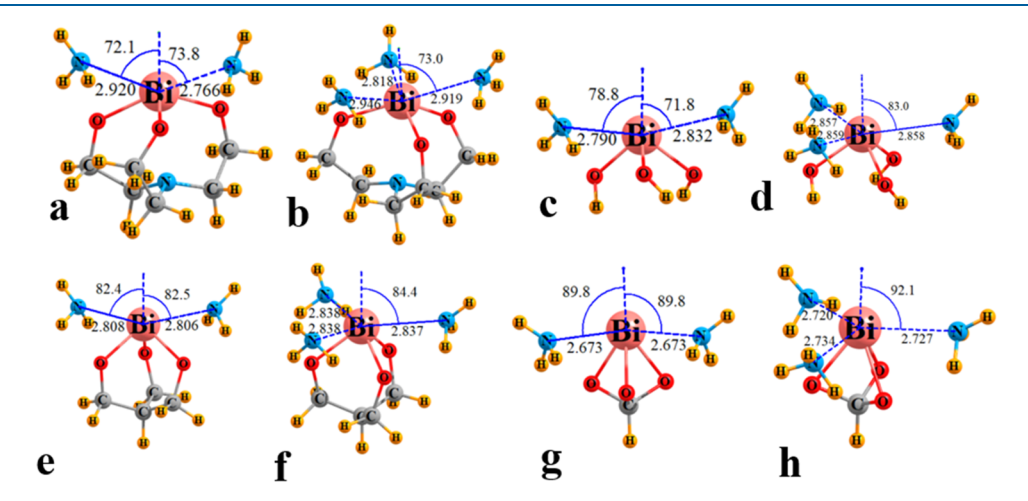


Figure 7. Optimized geometries of complexes containing two and three NH₃ with the Lewis acids (a, b) biatrane, (c, d) Bi(OH)₃, (e, f) Bi(OCH₂)₃CH, and (g, h) BiO₃CH. Distances in Å and angles in degs. The dashed blue line represents the C_3 rotation axis.

quantities for the Z(OH)₃ and Z(OCH₂)₃CH units with no or small strain, and then achieve their pinnacle for the highly pyramidal ZO₃CH in the last column. This ordering is consistent whether there is one base present, two, or three. Although As is capable of engaging in three simultaneous ZBs in most cases, the shallowness of its σ -hole in the atrane limits it to only one such bond. Given that the central Z atom acts as an electron acceptor in all of the ZBs present, it is unsurprising that the average bond energy declines with n but remains quite sizable even for 3 such bonds. Even with the decline in the average bond energy with n, the highly pyramidal coordination of the ZO₃CH units keeps this bond energy from sinking below 7 kcal/mol, even when there are three bonds present and when the Z atom is P. All told, the strongest bond of 20.3 kcal/mol is connected with the BiO₃CH system. As a point of comparison with experiment, Moaven et al. had recently measured⁴⁵ a ZB energy of 6 kcal/mol for Sb-atrane with an O electron donor. This value compares very well with the calculated value of 9.7 kcal/mol for the stronger N donor considered here.

Other manifestations of the presence of a σ -hole bond like those discussed here can be related to perturbations of the geometry and vibrational spectrum. Pursuant to the transfer of charge into the antibonding $\sigma^*(ZO)$ orbital of the Lewis acid, one would expect a weakening of this bond that would reveal itself as a stretch. The internal Z–O bond lengths in the Lewis acid units are contained in the first column of Table 7, which

Table 7. Effect of the Addition of NH₃ to Opposing Z–O Bond Lengths (Å) and Symmetric Stretching Frequency (cm⁻¹) within Lewis Acid

	r(Z-O)	Δr	ν	$\Delta \nu$
P-atrane	1.631		729.4	
$P(OH)_3$	1.636		834.7	
$P(OCH_2)_3CH$	1.634		785.6	
PO ₃ CH	1.687	0.057	777.8	-23.4
As-atrane	1.783	0.008	631.1	-19.2
$As(OH)_3$	1.778	0.019	739.2	-17.7
$As(OCH_2)_3CH$	1.776	0.012	689.7	-15.8
AsO ₃ CH	1.824	0.070	601.7	-19.4
Sb-atrane	1.974	0.012	571.0	-31.6
$Sb(OH)_3$	1.948	0.053	667.2	-18.2
$Sb(OCH_2)_3CH$	1.946	0.025	631.9	-24.1
SbO ₃ CH	1.991	0.061	533.3	-18.6
Biatrane	2.123	0.011	513.7	-26.5
$Bi(OH)_3$	2.049	0.051	609.1	-17.8
$Bi(OCH_2)_3CH$	2.044	0.029	583.6	-21.1
BiO ₃ CH	2.084	0.061	477.0	-12.2

shows first how the high degree of deformation of the ZO₃CH causes it to have a longer Z–O bond length than the other less strained species by some 0.04–0.05 Å. The converse sort of distortion, the flattening of the atranes, also result in bond elongation, albeit by not quite as much. More relevant, each such bond undergoes a stretch when NH₃ is positioned opposite to it, transferring charge into its antibonding orbital. These elongations are quite substantial and importantly gain in magnitude along with the higher degree of pyramidality, also associated with stronger ZBs. The symmetric stretching normal mode has a frequency on the order of 480–830 cm⁻¹ for these various Lewis acid monomers, as reported in Table 7, which drops as internal distortions are imposed, whether flattened or

more pyramidal. The imposition of a ZB with an NH_3 base red-shifts this frequency by amounts varying between 12 and 32 cm⁻¹. However, there is no obvious pattern governing the magnitude of this shift.

The geometries computed here are fully consistent with a number of relevant crystal structures. In particular, the internal $\alpha(OSbO)$ angle for $Sb(OH)_3$ is calculated to be 89.4° when it is complexed with three NH₃ bases. This value squares nicely with this same internal angle for three crystals where a Sb(OR)₃ unit is engaged in three external ZBs: 89.0° (PEDKUH), 43 88.9° (PEDLAO), 43 and 92.2° (FEPWUS). 41 A diffraction study of a molecule very much akin to $P(OCH_2)_3CH^{52}$ yielded an internal α angle of 101°, within 2° of the value computed here. The ZO₃CH molecules with their higher degree of pyramidality model a number of systems in the literature, spanning all of the pnicogen atoms from P to Bi, with the Z connected to either O or N atoms.⁸⁰⁻⁸⁵ The internal α angles of these units are as small as 80°, comparable to the optimized values for the ZO₃CH systems examined here.

In summary, the principles extracted from the artificial imposition of an opening or closing of the umbrella representing the arrangement around the Z atom are in full operation when the strain is a product of the internal bonding within the molecule. With a few exceptions, the central Z atom is fully capable of engaging in three simultaneous pnicogen bonds, which weaken only slightly as each new base is added. Whether participating in one or more ZBs, these bonds are strengthened very significantly in those molecules whose internal structure represents a highly pyramidal geometry and conversely weakened if distorted toward a flatter arrangement.

CONCLUSIONS

If one thinks of the three Z–X bonds to a central pnicogen atom as the ribs of an umbrella, a closing motion of the umbrella, which brings the X units closer to one another, acts to intensify the σ -holes on Z and strengthen its pnicogen bonds to nucleophiles. This effect can be quite sizable. For example, the ZB energies of the strained SbO₃CH and BiO₃CH model systems with NH₃ are 20 kcal/mol. The opposite effect of weakened ZBs results from an opening of the umbrella, as might arise in certain molecules like atranes containing larger rings. All of the Z atoms tested are capable of engaging in three ZBs simultaneously, with the sole exception of P, or As when in the flattened atrane configuration, which is limited to only one ZB.

ASSOCIATED CONTENT

Supporting Information

The Supporting Information is available free of charge at https://pubs.acs.org/doi/10.1021/acs.inorgchem.3c03141

Angular characteristics of optimized ZX₃ monomers; comparisons with experimental parameters; AIM, NBO, and SAPT parameters of their complexes with NH₃ when deformed; and Cartesian coordinates of all relevant monomers and dimers (PDF)

AUTHOR INFORMATION

Corresponding Author

Steve Scheiner – Department of Chemistry and Biochemistry, Utah State University, Logan, Utah 84322-0300, United

States; orcid.org/0000-0003-0793-0369; Email: steve.scheiner@usu.edu

Authors

Mariusz Michalczyk – Faculty of Chemistry, Wrocław University of Science and Technology, 50-370 Wrocław, Poland; oorcid.org/0000-0002-6495-6963

Wiktor Zierkiewicz — Faculty of Chemistry, Wrocław University of Science and Technology, 50-370 Wrocław, Poland; orcid.org/0000-0002-4038-5959

Complete contact information is available at: https://pubs.acs.org/10.1021/acs.inorgchem.3c03141

Note

The authors declare no competing financial interest.

ACKNOWLEDGMENTS

The authors are grateful to Dr. Anthony Cozzolino whose own work inspired these calculations and who kindly surveyed the literature for relevant crystal structures. The authors acknowledge the Academic Computing Centre Cyfronet-Kraków (Ares supercomputer, part of the PL-Grid infrastructure), Wrocław Center for Networking and Supercomputing (WCSS), for generous grants of computer time and facilities. This material was based upon work supported by the National Science Foundation under Grant No. 1954310 to SS.

REFERENCES

- (1) Joesten, M. D.; Schaad, L. J. *Hydrogen Bonding*; Marcel Dekker: New York, 1974; p 622.
- (2) Desiraju, G. R.; Steiner, T. The Weak Hydrogen Bond in Structural Chemistry and Biology; Oxford: New York, 1999; p 507.
- (3) Szczesniak, M. M.; Scheiner, S. Møller-Plesset treatment of electron correlation in (HOHOH)⁻. *J. Chem. Phys.* **1982**, 77, 4586–4593.
- (4) Cuma, M.; Scheiner, S.; Kar, T. Effect of adjoining aromatic ring upon excited state proton transfer. o-Hydroxybenzaldehyde. *J. Mol. Struct.* **1999**, *467*, 37–49.
- (5) Gilli, G.; Gilli, P. The Nature of the Hydrogen Bond; Oxford University Press: Oxford, UK, 2009; p 313.
- (6) Scheiner, S. Hydrogen Bonding: A Theoretical Perspective; Oxford University Press: New York, 1997; p 375.
- (7) Gleiter, R.; Werz, D. B.; Rausch, B. J. A World Beyond Hydrogen Bonds?—Chalcogen—Chalcogen Interactions Yielding Tubular Structures. *Chem. Eur. J.* **2003**, *9*, 2676–2683, DOI: 10.1002/chem.200204684.
- (8) Bleiholder, C.; Werz, D. B.; Koppel, H.; Gleiter, R. Theoretical investigations on chalcogen-chalcogen interactions: What makes these nonbonded interactions bonding? *J. Am. Chem. Soc.* **2006**, *128*, 2666–2674.
- (9) Wang, W.; Ji, B.; Zhang, Y. Chalcogen bond: A sister noncovalent bond to halogen bond. *J. Phys. Chem. A* **2009**, *113*, 8132–8135.
- (10) Bauzá, A.; Quiñonero, D.; Deyà, P. M.; Frontera, A. Halogen bonding versus chalcogen and pnicogen bonding: a combined Cambridge structural database and theoretical study. *CrystEngComm* **2013**, *15*, 3137–3144.
- (11) Fanfrlík, J.; Přáda, A.; Padělková, Z.; Pecina, A.; Macháček, J.; Lepšík, M.; Holub, J.; Růžička, A.; Hnyk, D.; Hobza, P. The Dominant Role of Chalcogen Bonding in the Crystal Packing of 2D/3D Aromatics. *Angew. Chem., Int. Ed.* **2014**, *53*, 10139–10142.
- (12) de Paul N Nziko, V.; Scheiner, S. Comparison of p-hole tetrel bonding with s-hole halogen bonds in complexes of XCN (X = F, Cl, Br, I) and NH₃. *Phys. Chem. Chem. Phys.* **2016**, *18*, 3581–3590, DOI: 10.1039/C5CP07545A.

- (13) Trujillo, C.; Sanchez-Sanz, G.; Alkorta, I.; Elguero, J. Halogen, chalcogen and pnictogen interactions in $(XNO_2)_2$ homodimers (X = F, Cl, Br, I). New J. Chem. **2015**, 39, 6791–6802.
- (14) Alkorta, I.; Sánchez-Sanz, G.; Elguero, J.; Del Bene, J. E. Influence of hydrogen bonds on the P···P pnicogen bond. *J. Chem. Theory Comput.* **2012**, *8*, 2320–2327.
- (15) Bauzá, A.; Quiñonero, D.; Deyà, P. M.; Frontera, A. Pnicogen—p complexes: theoretical study and biological implications. *Phys. Chem. Chem. Phys.* **2012**, *14*, 14061–14066.
- (16) Galmés, B.; Juan-Bals, A.; Frontera, A.; Resnati, G. Charge-Assisted Chalcogen Bonds: CSD and DFT Analyses and Biological Implication in Glucosidase Inhibitors. *Chem. Eur. J.* **2020**, *26*, 4599–4606, DOI: 10.1002/chem.201905498.
- (17) Clark, T.; Hennemann, M.; Murray, J. S.; Politzer, P. Halogen bonding: the s-hole. *J. Mol. Model.* **2007**, *13*, 291–296.
- (18) Mertsalov, D. F.; Gomila, R. M.; Zaytsev, V. P.; Grigoriev, M. S.; Nikitina, E. V.; Zubkov, F. I.; Frontera, A. On the Importance of Halogen Bonding Interactions in Two X-ray Structures Containing All Four (F, Cl, Br, I) Halogen Atoms. *Crystals* **2021**, *11*, No. 1406, DOI: 10.3390/cryst11111406.
- (19) Scheiner, S. Origins and properties of the tetrel bond. *Phys. Chem. Chem. Phys.* **2021**, 23, 5702–5717.
- (20) Palusiak, M.; Grabowski, S. J. Do intramolecular halogen bonds exist? Ab initio calculations and crystal structures' evidences. *Struct. Chem.* **2008**, *19*, 5–11.
- (21) Grabowski, S. J. Halogen bond and its counterparts: Bent's rule explains the formation of nonbonding interactions. *J. Phys. Chem. A* **2011**, *115*, 12340–12347.
- (22) Scheiner, S.; Hunter, S. Influence of Substituents in the Benzene Ring on the Halogen Bond of Iodobenzene with Ammonia. *ChemPhysChem* **2022**, 23, No. e202200011.
- (23) Cunha, A. V.; Havenith, R. W. A.; van Gog, J.; De Vleeschouwer, F.; De Proft, F.; Herrebout, W. The Halogen Bond in Weakly Bonded Complexes and the Consequences for Aromaticity and Spin-Orbit Coupling. *Molecules* **2023**, 28, No. 772, DOI: 10.3390/molecules28020772.
- (24) Azofra, L. M.; Scheiner, S. Tetrel, chalcogen, and CH·O hydrogen bonds in complexes pairing carbonyl-containing molecules with 1, 2, and 3 molecules of CO₂. *J. Chem. Phys.* **2015**, *142*, No. 034307.
- (25) Cavallo, G.; Metrangolo, P.; Milani, R.; Pilati, T.; Priimagi, A.; Resnati, G.; Terraneo, G. The Halogen Bond. *Chem. Rev.* **2016**, *116*, 2478–2601.
- (26) Scheiner, S. Sensitivity of Noncovalent Bonds to Intermolecular Separation: Hydrogen, Halogen, Chalcogen, and Pnicogen Bonds. *CrystEngComm* **2013**, *15*, 3119–3124.
- (27) Taylor, A. J.; Docker, A.; Beer, P. D. Allosteric and Electrostatic Cooperativity in a Heteroditopic Halogen Bonding Receptor System. *Chem. Asian J.* **2023**, *18*, No. e202201170, DOI: 10.1002/asia.202201170.
- (28) Jungbauer, S. H.; Huber, S. M. Cationic Multidentate Halogen-Bond Donors in Halide Abstraction Organocatalysis: Catalyst Optimization by Preorganization. *J. Am. Chem. Soc.* **2015**, *137*, 12110—12120.
- (29) Cozzolino, A. F.; Elder, P. J. W.; Lee, L. M.; Vargas-Baca, I. The role of the Lewis acid—base properties in the supramolecular association of 1,2,5-chalcogenadiazoles. *Can. J. Chem.* **2013**, *91*, 338–347.
- (30) Chakraborty, S.; Maji, S.; Ghosh, R.; Jana, R.; Datta, A.; Ghosh, P. Aryl-platform-based tetrapodal 2-iodo-imidazolium as an excellent halogen bond receptor in aqueous medium. *Chem. Commun.* **2019**, 55, 1506–1509.
- (31) Hein, R.; Beer, P. D. Halogen bonding and chalcogen bonding mediated sensing. *Chem. Sci.* **2022**, *13*, 7098–7125.
- (32) Docker, A.; Guthrie, C. H.; Kuhn, H.; Beer, P. D. Modulating Chalcogen Bonding and Halogen Bonding Sigma-Hole Donor Atom Potency and Selectivity for Halide Anion Recognition. *Angew. Chem., Int. Ed.* **2021**, *60*, 21973–21978.

- (33) Scheiner, S. Comparison of halide receptors based on H, halogen, chalcogen, pnicogen, and tetrel bonds. *Faraday Discuss*. **2017**, 203, 213–226.
- (34) Del Bene, J. E.; Alkorta, I.; Elguero, J. IR and NMR properties of N-base:PH₂F:BeX₂ ternary and corresponding binary complexes stabilised by pnicogen and beryllium bonds. *Mol. Phys.* **2021**, *119*, No. e1905191.
- (35) Bauzá, A.; Mooibroek, T. J.; Frontera, A. σ -Hole Opposite to a Lone Pair: Unconventional Pnicogen Bonding Interactions between ZF₃ (Z = N, P, As, and Sb) Compounds and Several Donors. ChemPhysChem **2016**, 17, 1608–1614.
- (36) Grabowski, S. J. Pnicogen and tetrel bonds—tetrahedral Lewis acid centres. *Struct. Chem.* **2019**, *30*, 1141–1152.
- (37) Alkorta, I.; Elguero, J.; Grabowski, S. J. Pnicogen and hydrogen bonds: complexes between PH₃X⁺ and PH₂X systems. *Phys. Chem. Chem. Phys.* **2015**, *17*, 3261–3272.
- (38) Moaven, S.; Andrews, M. C.; Polaske, T. J.; Karl, B. M.; Unruh, D. K.; Bosch, E.; Bowling, N. P.; Cozzolino, A. F. Triple-Pnictogen Bonding as a Tool for Supramolecular Assembly. *Inorg. Chem.* **2019**, 58, 16227–16235, DOI: 10.1021/acs.inorgchem.9b02761.
- (39) Trubenstein, H. J.; Moaven, S.; Vega, M.; Unruh, D. K.; Cozzolino, A. F. Pnictogen bonding with alkoxide cages: which pnictogen is best? *New J. Chem.* **2019**, *43*, 14305–14312.
- (40) Moaven, S.; Andrews, M. C.; Polaske, T. J.; Karl, B. M.; Unruh, D. K.; Bosch, E.; Bowling, N. P.; Cozzolino, A. F. Triple-Pnictogen Bonding as a Tool for Supramolecular Assembly. *Inorg. Chem.* **2019**, 58, 16227–16235.
- (41) Ensinger, U.; Schwarz, W.; Schrutz, B.; Sommer, K.; Schmidt, A. Methoxostibane. Struktur und Schwingungsspektren. *Z. Anorg. Allg. Chem.* **1987**, *544*, 181–191, DOI: 10.1002/zaac.19875440119.
- (42) Veith, M.; Yu, E.-C.; Huch, V. Synthesis and Structures of Alkali(alkoxy) Antimonates and Bismuthates. *Chem. Eur. J.* **1995**, *1*, 26–32, DOI: 10.1002/chem.19950010108.
- (43) Moaven, S.; Yu, J.; Yasin, J.; Unruh, D. K.; Cozzolino, A. F. Precise Steric Control over 2D versus 3D Self-Assembly of Antimony(III) Alkoxide Cages through Strong Secondary Bonding Interactions. *Inorg. Chem.* **2017**, *56*, 8372–8380.
- (44) Moaven, S.; Yu, J.; Vega, M.; Unruh, D. K.; Cozzolino, A. F. Self-assembled reversed bilayers directed by pnictogen bonding to form vesicles in solution. *Chem. Commun.* **2018**, *54*, 8849–8852.
- (45) Moaven, S.; Villanueva, O. H.; Unruh, D. K.; Cozzolino, A. F. The complicating role of pnictogen bond formation in the solution-phase and solid-state structures of the heavier pnictogen atranes. *Dalton Trans.* **2022**, *51*, 11335–11339.
- (46) Wysokiński, R.; Zierkiewicz, W.; Michalczyk, M.; Scheiner, S. How Many Pnicogen Bonds can be Formed to a Central Atom Simultaneously? *J. Phys. Chem. A* **2020**, *124*, 2046–2056.
- (47) Scheiner, S. Coordination of a Central Atom by Multiple Intramolecular Pnicogen Bonds. *Inorg. Chem.* **2020**, *59*, 9315–9324.
- (48) Wysokiński, R.; Zierkiewicz, W.; Michalczyk, M.; Scheiner, S. Competition between Intra and Intermolecular Pnicogen Bonds: Complexes between Naphthalene Derivatives and Neutral or Anionic Bases. *ChemPhysChem* **2022**, 23, No. e202200173, DOI: 10.1002/cphc.202200173.
- (49) Scheiner, S.; Michalczyk, M.; Zierkiewicz, W. Involvement of Arsenic Atom of AsF₃ in Five Pnicogen Bonds: Differences between X-ray Structure and Theoretical Models. *Molecules* **2022**, 27, No. 6486, DOI: 10.3390/molecules27196486.
- (50) Verkade, J.; Reynolds, L. Notes- The Synthesis of a Novel Ester of Phosphorus and of Arsenic. J. Org. Chem. 1960, 25, 663–665.
- (51) Milbrath, D. S.; Springer, J. P.; Clardy, J. C.; Verkade, J. G. Phosphorus ester basicity dependence on constraint. Crystal and molecular structures of P(OCH₂)₃CCH₂Br and O:P(OCH₂)₂C-(CH₃)O. *J. Am. Chem. Soc.* **1976**, 98, 5493–5496.
- (52) Albright, J. O.; Clardy, J. C.; Verkade, J. G. Crystal and molecular structure of pentakis(4-methyl-1-phospha-2,6,7-trioxabicyclo[2.2.2]octane)cobalt(I)(acetonitrile)trinitratocobalt(II), {Co[P(OCH2)3CMe]5}[Co(NO3)3NCMe]. *Inorg. Chem.* 1977, 16, 1575–1580.

- (53) Jansen, M.; Moebs, M. Structural investigations on solid tetraphosphorus hexaoxide. *Inorg. Chem.* **1984**, 23, 4486–4488.
- (54) Pike, R. D.; Reinecke, B. A.; Dellinger, M. E.; Wiles, A. B.; Harper, J. D.; Cole, J. R.; Dendramis, K. A.; Borne, B. D.; Harris, J. L.; Pennington, W. T. Bicyclic Phosphite Esters from Pentaerythritol and Dipentaerythritol: New Bridging Ligands in Organometallic and Inorganic Chemistry. *Organometallics* **2004**, 23, 1986–1990.
- (55) Tanski, J. M.; Kelly, B. V.; Parkin, G. Multidentate aryloxide and oxo-aryloxide complexes of antimony: synthesis and structural characterization of $[\eta 4\text{-N}(o\text{-C6H4O})3]\text{Sb}(OSMe2)$, $\{\{[\eta 3\text{-N}(o\text{-C6H4OH})(o\text{-C6H4O})2]\text{Sb}\}2(\mu 2\text{-O})\}2$ and $\{[\eta 3\text{-PhN}(o\text{-C6H4O})2]\text{Sb}\}4(\mu 3\text{-O})2$. Dalton Trans. **2005**, 2442–2447.
- (56) Frisch, M. J.; Trucks, G. W.; Schlegel, H. B.; Scuseria, G. E.; Robb, M. A.; Cheeseman, J. R.; Scalmani, G.; Barone, V.; Petersson, G. A.; Nakatsuji, H.; Li, X.; Caricato, M.; Marenich, A. V.; Bloino, J.; Janesko, B. G.; Gomperts, R.; Mennucci, B.; Hratchian, H. P.; Ortiz, J. V.; Izmaylov, A. F.; Sonnenberg, J. L.; Williams-Young, D.; Ding, F.; Lipparini, F.; Egidi, F.; Goings, J.; Peng, B.; Petrone, A.; Henderson, T.; Ranasinghe, D.; Zakrzewski, V. G.; Gao, J.; Rega, N.; Zheng, G.; Liang, W.; Hada, M.; Ehara, M.; Toyota, K.; Fukuda, R.; Hasegawa, J.; Ishida, M.; Nakajima, T.; Honda, Y.; Kitao, O.; Nakai, H.; Vreven, T.; Throssell, K.; Montgomery, J. A., Jr.; Peralta, J. E.; Ogliaro, F.; Bearpark, M. J.; Heyd, J. J.; Brothers, E. N.; Kudin, K. N.; Staroverov, V. N.; Keith, T. A.; Kobayashi, R.; Normand, J.; Raghavachari, K.; Rendell, A. P.; Burant, J. C.; Iyengar, S. S.; Tomasi, J.; Cossi, M.; Millam, J. M.; Klene, M.; Adamo, C.; Cammi, R.; Ochterski, J. W.; Martin, R. L.; Morokuma, K.; Farkas, O.; Foresman, J. B.; Fox, D. J. Gaussian 16, Rev. C.01; Gaussian, Inc.: Wallingford, CT, 2016.
- (57) Zhao, Y.; Truhlar, D. G. The M06 suite of density functionals for main group thermochemistry, thermochemical kinetics, non-covalent interactions, excited states, and transition elements: two new functionals and systematic testing of four M06-class functionals and 12 other functionals. *Theor. Chem. Acc.* 2008, 120, 215–241.
- (58) Vamhindi, B. S. D. R.; Karton, A. Can DFT and ab initio methods adequately describe binding energies in strongly interacting C_6X_6 :" C_2X_n $\pi-\pi$ complexes? *Chem. Phys.* **2017**, 493, 12–19.
- (59) Podeszwa, R.; Szalewicz, K. Density functional theory overcomes the failure of predicting intermolecular interaction energies. *J. Chem. Phys.* **2012**, *136*, No. 161102, DOI: 10.1063/1.4707166.
- (60) Karthikeyan, S.; Ramanathan, V.; Mishra, B. K. Influence of the substituents on the CH⁻⁻p interaction: Benzene—methane complex. *J. Phys. Chem. A* **2013**, *117*, 6687–6694.
- (61) Majumder, M.; Mishra, B. K.; Sathyamurthy, N. CH"p and p"p interaction in benzene-acetylene clusters. *Chem. Phys.* **2013**, *557*, 59–65, DOI: 10.1016/j.cplett.2012.12.027.
- (62) Vincent, M. A.; Hillier, I. H. The structure and interaction energies of the weak complexes of CHClF₂ and CHF₃ with HCCH: A test of density functional theory methods. *Phys. Chem. Chem. Phys.* **2011**, *13*, 4388–4392.
- (63) Boese, A. D. Density Functional Theory and Hydrogen Bonds: Are We There Yet? *ChemPhysChem* **2015**, *16*, 978–985.
- (64) Walker, M.; Harvey, A. J. A.; Sen, A.; Dessent, C. E. H. Performance of M06, M06-2X, and M06-HF Density Functionals for Conformationally Flexible Anionic Clusters: M06 Functionals Perform Better than B3LYP for a Model System with Dispersion and Ionic Hydrogen-Bonding Interactions. *J. Phys. Chem. A* 2013, 117, 12590–12600.
- (65) Molnar, L. F.; He, X.; Wang, B.; Merz, K. M. Further analysis and comparative study of intermolecular interactions using dimers from the S22 database. *J. Chem. Phys.* **2009**, *131*, No. 065102.
- (66) Boys, S. F.; Bernardi, F. The calculation of small molecular interactions by the differences of separate total energies. Some procedures with reduced errors. *Mol. Phys.* **1970**, *19*, 553–566.
- (67) Lu, T.; Chen, F. Multiwfn: A multifunctional wavefunction analyzer. J. Comput. Chem. 2012, 33, 580-592.
- (68) Bader, R. F. W. Atoms in Molecules, A Quantum Theory; Clarendon Press: Oxford, 1990; Vol. 22, p 438.

- (69) Keith, T. A. AIMAll; TK Gristmill Software: Overland Park KS, 2013.
- (70) Reed, A. E.; Weinhold, F. Natural bond orbital analysis of near Hartree-Fock water dimer. *J. Chem. Phys.* **1983**, 78, 4066–4073.
- (71) Reed, A. E.; Weinhold, F.; Curtiss, L. A.; Pochatko, D. J. Natural bond orbital analysis of molecular interactions: Theoretical studies of binary complexes of HF, H₂O, NH₃, N₂, O₂, F₂, CO and CO₂ with HF, H₂O, and NH₃. *J. Chem. Phys.* **1986**, *84*, 5687–5705.
- (72) Szalewicz, K.; Jeziorski, B. Symmetry-Adapted Perturbation Theory of Intermolecular Interactions. In *Molecular Interactions. From Van der Waals to Strongly Bound Complexes*; Scheiner, S., Ed.; Wiley: New York, 1997; pp 3–43.
- (73) Moszynski, R.; Wormer, P. E. S.; Jeziorski, B.; van der Avoird, A. Symmetry-adapted perturbation theory of nonadditive three-body interactions in van der Waals molecules. I. General theory. *J. Chem. Phys.* **1995**, *103*, 8058–8074.
- (74) Smith, D. G. A.; Burns, L. A.; Simmonett, A. C.; Parrish, R. M.; Schieber, M. C.; Galvelis, R.; Kraus, P.; Kruse, H.; Remigio, R. D.; Alenaizan, A.; James, A. M.; Lehtola, S.; Misiewicz, J. P.; Scheurer, M.; Shaw, R. A.; Schriber, J. B.; Xie, Y.; Glick, Z. L.; Sirianni, D. A.; O'Brien, J. S.; Waldrop, J. M.; Kumar, A.; Hohenstein, E. G.; Pritchard, B. P.; Brooks, B. R.; Schaefer, H. F., III; Sokolov, A. Y.; Patkowski, K.; DePrince, A. E., III; Bozkaya, U.; King, R. A.; Evangelista, F. A.; Turney, J. M.; Crawford, T. D.; Sherrill, C. D. PSI4 1.4: Open-source software for high-throughput quantum chemistry. J. Chem. Phys. 2020, 152, No. 184108, DOI: 10.1063/5.0006002.
- (75) Konaka, S.; Masao, K. Determination of the Molecular Structures of AsF₃ and AsCl₃ by Gas Electron Diffraction. *Bull. Chem. Soc. Jpn.* **1970**, *43*, 1693–1703.
- (76) Webster, M.; Keats, S. Crystal structure of arsenic trichloride—trimethylamine, AsCl₃,NMe₃. *J. Chem. Soc. A* **1971**, *0*, 836–838.
- (77) Hulme, R.; Scruton, J. C. The crystal structure of 1:1 antimony trichloride—aniline, SbCl₃, C₆H₅NH₂. *J. Chem. Soc. A* **1968**, *0*, 2448—2452.
- (78) Adhikari, U.; Scheiner, S. Sensitivity of pnicogen, chalcogen, halogen and H-bonds to angular distortions. *Chem. Phys. Lett.* **2012**, 532, 31–35.
- (79) Scheiner, S. The pnicogen bond: Its relation to hydrogen, halogen, and other noncovalent bonds. *Acc. Chem. Res.* **2013**, *46*, 280–288.
- (80) Bullivant, D. P.; Dove, M. F. A.; Haley, M. J. Determination of the molecular structure and absolute configuration of (R)-tris-(trifluoroacetato)antimony(III). *J. Chem. Soc. Dalton Trans.* **1980**, 105–108.
- (81) Mattes, R.; Rühl, D. Darstellung und Struktur von Antimon-(III)-tris(thiophosphinaten). Z. Anorg. Allg. Chem. 1984, 508, 19–25.
- (82) Kou, X.; Wang, X.; Mendoza-Espinosa, D.; Zakharov, L. N.; Rheingold, A. L.; Watson, W. H.; Brien, K. A.; Jayarathna, L. K.; Hanna, T. A. Bismuth Aryloxides. *Inorg. Chem.* **2009**, *48*, 11002–11016.
- (83) Kleemann, S.; Fluck, E.; Schwarz, W. ÜBER DIAZADIPHOS-PHETIDINE IV Synthese und Struktur von 1.3-Dimethyl-2-methylamino-4-diethylamino-2-oxo-1.3.2.4-diaza-λ5,λ3-diphosphetidin. *Phosphorus Sulfur Relat. Elem.* **1981**, *12*, 19–25.
- (84) Hering, C.; Rothe, J.; Schulz, A.; Villinger, A. Structure and Bonding of Novel Acyclic Bisaminoarsenium Cations. *Inorg. Chem.* **2013**, *52*, 7781–7790.
- (85) Beswick, M. A.; Cromhout, N. L.; Harmer, C. N.; Paver, M. A.; Raithby, P. R.; Rennie, M.-A.; Steiner, A.; Wright, D. S. Assembly of Mixed-Metal Cages Using Polyimido Antimony(III) Anions. Syntheses and Structures of $[Sb_3(NCy)_4(HNCy)_2]K\cdot 2(toluene)$, $[Sb_2(NCy)_4]_2M_4$ (M = Cu, Ag), and $[Sb(NCy)_3]_2Pb_3$ (Cy = Cyclohexyl, C_6H_{11}). Inorg. Chem. 1997, 36, 1740–1744.